Published in final edited form as:
Bioconjug Chem. 2009 May 20; 20(5): 888–894. doi:10.1021/bc800433y.

Synthesis and characterization of an ^{111}In-labeled peptide for the in vivo localization of human cancers expressing the urokinase-type plasminogen activator receptor (uPAR)

Dijie Liu[†,#], **Douglas Overbey**[†,#], **Lisa Watkinson**[†,#], and **Michael F. Giblin**[†,‡,#,*]

[†]Research Service, Harry S. Truman Memorial Veterans' Administration Hospital, Columbia, MO 65201.

[#]The Radiopharmaceutical Sciences Institute, University of Missouri-Columbia, Columbia, MO 65211.

[‡]Department of Radiology, University of Missouri-Columbia School of Medicine, Columbia, MO 65211.

Abstract

This study describes the synthesis and preliminary biologic evaluation of an ^{111}Inlabeled peptide antagonist of the urokinase-type plasminogen activator receptor (uPAR) as a potential probe for assessing metastatic potential of human breast cancer in vivo. The peptide (NAc-dD-CHA-F-dS-dR-Y-L-W-S-βAla)$_2$-K-K(DOTA)-NH$_2$ was synthesized and conjugated with the DOTA chelating moiety via conventional Solid-Phase Peptide Synthesis (SPPS), purified by reversed-phase HPLC, and characterized by MALDI-TOF MS and receptor binding assay. In vitro receptor binding studies demonstrated an IC_{50} of 240 ± 125 nM for the peptide, compared with IC_{50}'s of 0.44 ± 0.02 and 0.75 ± 0.01 nM for the amino terminal fragment (ATF) of the urokinase-type plasminogen activator (uPA) and full-length uPA, respectively. In vivo biodistribution studies were carried out using SCID mice bearing MDA-MB-231 human breast cancer xenografts. Biodistribution data was collected at 1, 4, and 24 hr post-injection of ^{111}In-DOTA-peptide, and compared with data obtained using a scrambled control peptide, as well as with data obtained using wild-type ATF radiolabeled with I-125. Biodistribution studies showed rapid elimination of the ^{111}In-labeled peptide from the blood pool, with 0.12 ± 0.06% ID/g remaining in blood at 4 hr pi. Elimination was seen primarily via the renal/urinary route, with 83.9 ± 2.2%ID in the urine at the same timepoint. Tumor uptake at this time was 0.53 ± 0.11%ID/g, resulting in tumor: blood and tumor: muscle ratios of 4.2 and 9.4, respectively. Uptake in tumor was significantly higher than that obtained using a scrambled control peptide that showed no specific binding to uPAR ($p < 0.05$). In vitro and ex vivo results both suggested that the magnitude of tumor-specific binding was reduced in this model by endogenous expression of uPA. The results indicate that radiolabeled peptide uPAR antagonists may find application in the imaging and therapy of uPAR-expressing breast cancers in vivo.

INTRODUCTION

The urokinase-type plasminogen activator (uPA) system plays an important role in the progression of many types of cancer (1–4). Binding of uPA to its receptor (uPAR) initiates a proteolytic cascade that ultimately results in degradation of extracellular matrix (ECM) components and activation of matrix metalloproteases (MMP's). These processes in turn lead

*Author to whom correspondence should be addressed: Michael F. Giblin, Ph.D., Research Service, A004 HSTMVH, 800 Hospital Dr. Columbia, MO 65201, USA. E-mail: GiblinM@health.missouri.edu Phone: 573-814-6000 x53669, Fax: 573-882-6129.

to tumor invasion and metastasis. Components of the uPA system, including uPAR, are overexpressed in various cancers, including human breast, prostate, and colorectal cancer, and overexpression is correlated with poor prognosis due to increased rates of metastatic relapse (5–11). The proven correlation between uPAR expression and metastatic potential provides an opportunity to develop an *in vivo* imaging agent which can both help define a subset of breast cancer patients at increased risk for metastatic disease and localize and ultimately treat metastatic disease.

Seminal research by Blasi, Ploug, and others (1,2,4,12–15) has clarified the functional elements of uPAR that are required for its interaction with uPA and with other proteins, including integrins and fibrinogen. uPA is a 54 kDa glycosylated serine protease that catalyzes the conversion of plasminogen to plasmin. Binding of pro-uPA to uPAR (CD87) results in proteolytic activation, yielding two-chain high molecular weight uPA (tc-HMW-uPA). uPAR is a glycosylphosphatidylinositol (GPI)-anchored receptor for uPA, and serves to concentrate uPA activity at the invasive front of tumor masses. Human uPAR is a 283 amino acid single chain protein, and is a member of the Ly-6/uPAR/α-neurotoxin family of proteins. In structure, it is arranged into three finger-like domains that enfold the uPA ligand within a central binding cavity. Binding of uPA to uPAR in this fashion serves to focalize uPA activity in such a way as to facilitate invasion of uPAR-expressing cancers by activation of a proteolytic cascade that breaks down extracellular matrix components and allows cancer cell migration into vasculature and lymphatics (2).

The aim of this study was to investigate the applicability of radiolabeled uPA antagonists to the detection of uPAR-expressing cancers in vivo. A series of small peptide inhibitors of the uPA-uPAR interaction have previously been developed (15), which demonstrate high affinity for uPAR. We have synthesized and characterized one such inhibitor, modified to contain a C-terminal DOTA chelating moiety, labeled the resulting compound with ^{111}In, and compared its in vivo biodistribution profile to that of ^{125}I-ATF using SCID mice bearing MDA-MB-231 human breast cancer tumor xenografts.

MATERIALS AND METHODS

Materials

ATF was obtained from American Diagnostica, Inc. Na^{125}I was obtained from Perkin Elmer. DOTA-mono-NHS-ester and Fmoc-L-Lys-mono-amide-DOTA-tris (tBu ester) were obtained from Macrocyclics, Inc. Rink Amide MBHA peptide synthesis resin and protected Fmoc-amino acids were obtained from Novabiochem. MALDI-TOF mass spectral analyses were performed by the Proteomics Center at the University of Missouri-Columbia. $^{111}InCl_3$ was obtained from Mallinckrodt Medical, Inc. as a 0.05N HCl solution. MDA-MB-231 cells were obtained from the American Type Culture Collection (ATCC). SiRNA's and anti-urokinase antibodies were obtained from Santa Cruz Biotechnology. All solvents were either ACS certified or HPLC grade, obtained from Fisher Scientific and used as received. Other reagents were purchased from Aldrich Chemical Company, Gibco, and Pierce.

Peptide synthesis and purification

Peptides were synthesized by standard solid phase peptide synthesis (SPPS) techniques, employing Fmoc protected amino acids and either DOTA-mono-NHS-ester or Fmoc-LLys-mono-amide-DOTA-tris (tBu ester) as building blocks. Polypeptides were assembled on Rink Amide MBHA resin, acetylated via HoBT/DCC activation of 5-fold excess acetic acid in 3:1 NMP:DMSO, then cleaved from the resin and deprotected using a 36:2:1:1 mixture of TFA:thioanisole:water:ethanedithiol. The addition of DOTA-mono-NHS-ester to the ε-amino group of the C-terminal lysine residue of (NAc-dD-CHA-F-dSdR-Y-L-W-S-βAla)$_2$-K-K-

NH_2 was carried out 0.1 M Na_2HPO_4, pH 8 for 3.5 hr at room temperature, using a 10–20-fold excess of DOTA NHS ester.

DOTA-conjugated peptides were purified by high performance liquid chromatography (HPLC). HPLC was performed on a Shimadzu system equipped with an SPD-20A UV detector and an in-line sodium iodide crystal radiometric detector. HPLC solvents consisted of H_2O containing 0.1% trifluoroacetic acid (Solvent A) and acetonitrile containing 0.1% trifluoroacetic acid (Solvent B). Conditions: A Phenomenex Jupiter C-18 (5 μm, 300 Å, 4.6 × 250 mm) column was used with a flow rate of 1.5 ml/min. Gradient purification of all compounds was achieved during a linear 30 minute ramp from 35% B to 45% B, followed by column rinse and reequilibration.

Radiolabeling

For the synthesis of ^{111}In-labeled compounds, aliquots of $^{111}InCl_3$ (0.2 – 2.5 mCi, 7.4 – 92.5 MBq, 4 – 50 μl) were added to solutions of (NAc-dD-CHA-F-dS-dR-YLWS-βAla)$_2$-K-K (DOTA)-NH_2 and scrambled negative control peptide (NAc-dD-W-dS-LY-dR-FS-CHA-βAla)$_2$-K-K(DOTA)-NH_2 (10 – 20 μg) in 0.4M ammonium acetate (200 μl). The pH of the reaction mixture was adjusted to 6.0. The reaction mixture was incubated for 1 hour at 80 °C. After 1 hour, an aliquot of 0.002M EDTA (50 μl) was added to the reaction mixture to complex unreacted $^{111}In^{3+}$. The resulting conjugates were purified to homogeneity by RP-HPLC. The ^{111}In-metallated conjugates eluted between 0.5 – 1.5 minutes after the associated non-metallated species. Purified ^{111}In-DOTA conjugates were then concentrated by passing through a 3M Empore C-18 HD high performance extraction disk (7mm/3ml) cartridge and eluting with 100% ethanol (400 μl). The concentrated fractions were immediately diluted 2-fold by addition of 0.1M NaH_2PO_4, then reduced in volume under a stream of $N_{2(g)}$, and finally diluted with 0.1M NaH_2PO_4 buffer, pH 7.0, to a final activity of approximately 2 μCi/ 100 μl.

The amino terminal fragment of uPA was iodinated essentially according to a previously published protocol (13). Briefly, 2–10 μg of the Amino Terminal Fragment of uPA (ATF) was iodinated using 0.2–1 mCi $Na^{125}I$ following ^{125}I activation using Iodogen precoated tubes (Pierce). After a 10-minute incubation in 25 mM Tris, 0.4 M NaCl, pH 7.5, the reaction was quenched by addition of excess free tyrosine and purified by fractionation on a D-Salt size exclusion cartridge (Pierce).

In vitro/Ex vivo receptor binding assays

Binding affinity of urokinase antagonists was measured by competition against ^{125}-IATF using whole MDA-MB-231 human breast cancer cells. Prior to incubations of peptide competitors and radiolabeled tracer with whole cells, cells were briefly rinsed with 50 mM glycine HCl, 100 mM NaCl, pH 3.0, then neutralized with 0.2 volume 0.5 M HEPES, 100 mM NaCl, pH 7.4, to strip away endogenous uPA. Cells were then rinsed and suspended in binding buffer, PBS/0.2% BSA, pH 7.4. 3×10^6 cells suspended in binding buffer were incubated at 37°C for 1 hr in presence of approximately 20–30,000 cpm ^{125}I-ATF and increasing concentrations of unlabeled peptide competitors. After the incubation, the reaction medium was aspirated and cells were washed three times with binding buffer. The radioactivity bound to the cells was counted in a Packard Riastar gamma counting system. Experiments were performed in triplicate and average values were used for the calculations. The specific activity of the tracer was 50–100 μCi/μg.

SiRNA studies

MDA-MB-231 cells were maintained in RPMI 1640 supplemented with 10% FBS, 2 mM L-Glutamine, 1 mM Sodium pyruvate, 10 mM HEPES, 0.1 mM MEM non-essential amino acids, and 50 μg/ml gentamicin. SiRNA transfections were performed using lipofectamine 2000

(Invitrogen) according to the manufacturer's instructions. Briefly, 2×10^5 MDA-MB-231 cells were seeded in 6-well plates in antibiotic-free medium and reached 30–50% confluence by the time of transfection. 40 pmol uPA siRNA (Santa Cruz Biotechnology) /5μl lipofectamine 2000 transfection complexes were added to each well and incubated at 37°C for 4 hours. Control siRNA (Santa Cruz Biotechnology) and notransfection controls were run in parallel. Each assay was performed in triplicate. 48 hours post-transfection, effectiveness of siRNA knockdown was assessed by receptor binding assay without acid stripping of endogenous uPA, western blot, and RT-PCR.

Immunoblot analysis

Whole cell MDA-MB-231 lysates were prepared 48 hrs post-transfection and separated by 10% SDS-PAGE, followed by transfer to a PVDF membrane. Loading volumes were normalized based on cell number equivalents. After blocking in 5% non-fat milk, 0.1% Tween-20, Tris-buffered saline (TTBS) at RT for 1 hr, membranes were probed with primary antibodies in blocking solution for 1 hr at RT, followed by extensive washing in TTBS. Goat anti-rabbit and goat anti-mouse IgG-HRP (Santa Cruz Biotechnology) were used for detection of immunoreactive proteins by chemiluminescence. Primary antibodies used were rabbit anti-uPA and mouse anti-β-actin (Santa Cruz Biotechnology).

Reverse transcription-PCR analysis

Total RNA from MDA-MB-231 cells 48 hr post-siRNA transfection was extracted using Tri-reagent (Molecular Research Center) and the Qiagen RNeasy kit. 5μg of total RNA was applied to synthesize first-strand cDNA using SuperScript reverse transcriptase III (Invitrogen), and PCR was performed in a 25 μl total volume containing 12.5 pmol of primers. The following primers were used: uPA sense 5'-TGC GTC CTG GTC GTG AGC GC-3' and uPA antisense 5'-CTA CAG CGC TGA CAC GCT TG-3' to amplify a 780-bp uPA fragment after 35 cycles at 94°C for 1 min, 55°C for 1 min, 72 °C for 1 min (31). For control GAPDH, the following primers were used: sense 5'-CTT CAT TGA CCT CAACAT GGT TT-3' and antisense 5'-GGC ATT GCT GAT GAT CTT GAG G-3' to amplify a 346-bp GAPDH fragment after 23 cycles of 94°C for 30 seconds, 63°C for 30 seconds, 72 °C for 1 min.

Biodistribution studies

Four- to 5-week old female ICR SCID (severe combined immunodeficient) outbred mice were obtained from Taconic (Germantown, NY). The mice were housed four animals per cage in sterile micro isolator cages in a temperature- and humidity-controlled room with a 12-hour light/12-hour dark schedule. The animals were fed sterile rodent chow (Ralston Purina Company, St. Louis, MO) and water *ad libitum*. Animals were housed one week prior to inoculation of tumor cells and anesthetized for injections with isoflurane (Baxter Healthcare Corp., Deerfield, IL) at a rate of 2.5% with 0.5L/min oxygen through a non-rebreathing anesthesia vaporizer.

MDA-MB-231 human breast cancer cells were injected on the bilateral subcutaneous (s.c.) flank with ~5×10^6 cells in a suspension of 100 μl 3:1 PBS:Matrigel per injection site. MDA-MB-231 cells were allowed to grow *in vivo* four to five weeks post inoculation, developing tumors ranging in sizes from 0.06 – 0.53 grams. The biodistribution and uptake of (NAc-dD-CHA-F-dS-dR-YLWS-βAla)$_2$-K-K(^{111}In-DOTA)-NH_2, scrambled negative control peptide (NAc-dD-W-dS-LY-dR-FS-CHA- βAla)$_2$-K-K(^{111}In-DOTA)-NH_2, and ^{125}I-ATF in tumor bearing SCID mice was studied. The mice (average weight, 25 g) were injected with aliquots (50–100 μl) of the radiolabeled peptide solution (55–90 kBq) *via* the tail vein. Tissues, organs and tumors were excised from animals sacrificed at 1, 4, and 24 hr p.i., weighed, and counted. Radioactivity was measured in a Wallac 1480 automated gamma counter and the percentinjected dose per gram tissue was calculated. Differences in organ uptake between the

two ^{111}In-labeled peptides were analyzed by Student's t test. Differences at the 95% confidence level ($P < 0.05$) were considered significant. Animal studies were conducted in accordance with the highest standards of care as outlined in the NIH Guide for Care and Use of Laboratory Animals and the Policy and Procedures for Animal Research at the Harry S. Truman Memorial Veterans' Hospital and according to approved protocols.

RESULTS

Synthesis and In Vitro Characterization

The peptides (NAc-dD-CHA-F-dS-dR-Y-L-W-S-βAla)$_2$-K-K(DOTA)-NH$_2$ (Figure 1) and (NAc-dD-W-dS-L-Y-dR-F-S-CHA-βAla)$_2$-K-K(DOTA)-NH$_2$ were synthesized by standard solid phase peptide synthesis techniques, utilizing two distinct synthetic routes. In the first instance, (NAc-dD-CHA-F-dS-dR-Y-L-W-S-βAla)$_2$-K-K(DOTA)-NH$_2$ was synthesized using a Boc-protected ε-amino group on the C-terminal lysine residue. Following addition of the N-terminal d-aspartic acid residue, the Fmoc-peptide was acetylated on resin via HoBT/DCC activation of 5-fold excess acetic acid in 3:1 NMP:DMSO. Following acetylation, the peptide was cleaved from the resin in a standard deprotection/cleavage mixture, and the free amino group of the C-terminal lysine was conjugated to an activated NHS ester of DOTA. In the second route, the scrambled negative control peptide (NAc-dD-W-dS-L-Y-dR-F-S-CHA-βAla)$_2$-K-K(DOTA)-NH$_2$ was synthesized using preconjugated Fmoc-L-Lys-mono-amide-DOTA-tris(t-Bu ester), followed by acetylation with HoBT/DCC activated acetic acid, and cleavage from the resin. In each case, the final products were purified by C18 RP HPLC, and masses were confirmed by MALDI-TOF MS (Table 1, Figure 2).

The peptide (NAc-dD-CHA-F-dS-dR-Y-L-W-S-βAla)$_2$-K-K(DOTA)-NH$_2$ contains a core uPAR-binding sequence (dD-CHA-F-dS-dR-Y-L-W-S) originally developed using phage display and combinatorial chemistry techniques (14,15). The affinity of this peptide construct for uPAR was measured using MDA-MB-231 human breast cancer cells and ^{125}I-labeled ATF. The ability of (NAc-dD-CHA-F-dS-dR-Y-L-W-S-βAla)$_2$-K-K(DOTA)-NH$_2$ to competitively displace ^{125}I-ATF from intact cells was 300–600-fold lower than that of either uPA or ATF, indicating that the dimeric peptide has relatively low affinity for uPAR (Figure 3, Table 1). The effect of scrambling the peptide sequence was to completely abolish competitive displacement of ATF (Figure 3), demonstrating the specific nature of (NAc-dD-CHA-F-dS-dR-Y-L-W-S-βAla)$_2$-K-K(DOTA)-NH$_2$ binding to uPAR.

Biodistribution

In vivo biodistribution studies were carried out using SCID mice bearing MDA-MB-231 human breast cancer tumor xenografts. Animals were injected with ^{111}In-labeled peptides and sacrificed 1, 4, and 24 hr post-injection (Table 2). Both the uPAR-targeting peptide and the scrambled control peptide cleared rapidly from the bloodstream, primarily via the renal/urinary route. At 4 hr pi, uptake of (NAc-dD-CHA-F-dS-dR-Y-LW-S-βAla)$_2$-K-K(^{111}In-DOTA)-NH$_2$ in blood and muscle were 0.12 ± 0.06 %ID/g and 0.06 ± 0.02 %ID/g respectively, while uptake in tumor was 0.53 ± 0.11 %ID/g. For comparison, uptake of the matched scrambled control peptide in blood and muscle were 0.15 ± 0.04 %ID/g and 0.12 ± 0.02 %ID/g respectively at this timepoint, while tumor uptake dropped significantly ($p < 0.05$) to 0.36 ± 0.05 %ID/g.

In vivo results obtained using ^{111}In-labeled peptide uPA antagonists were compared to those obtained using ^{125}I-labeled ATF, a molecule with an approximately 600-fold higher affinity for uPAR. As shown in table 3, tumor uptake of ^{125}I-ATF only exceeded blood levels at 24 hr pi, although this did not reach significant levels. At this timepoint, however, tumor uptake was significantly lowered by co-injection of excess unlabeled ATF ($p < 0.05$), again demonstrating the specific nature of the tumor uptake observed.

Ex vivo/In vitro studies

To address the issue of uPAR binding capacity in the SCID/MDA-MB-231 model system used here, tumor xenografts were excised from SCID mice following 4–5 weeks of in vivo growth and assayed for ^{125}I-ATF binding with or without stripping of endogenous uPA. Figure 4 demonstrates that specific binding of uPAR-targeted ligands is decreased 4–5 fold due to receptor occupancy by endogenously produced uPA.

To further demonstrate that uPAR-targeted agents could be used to quantify uPA binding sites, we used a uPA-specific set of siRNA's to specifically knock down uPA expression in MDA-MB-231 cells. As seen in Figure 5, Binding of ^{125}I-uPA to MDAMB-231 cells is significantly increased ($p < 0.01$) approximately 4.4-fold following siRNA-mediated knockdown of endogenous uPA in an in vitro model system. This increase in specific binding is correlated with decreases in both uPA mRNA and protein expression as determined by RT-PCR and western blot (Figure 5).

DISCUSSION

In this study, the synthesis and characterization of a low molecular weight peptide uPAR antagonist with an appended DOTA chelating moiety was described. This construct specifically displaced ^{125}I-labeled ATF with an IC_{50} of 240 ± 125 nM, a characteristic that was completely lost upon alteration of the primary peptide sequence employed. The affinity of (NAc-dD-CHA-F-dS-dR-Y-L-W-S-βAla)$_2$-K-K(DOTA)-NH_2 for uPAR was lower than expected from previously published data obtained for related constructs (15–17). This is due to a number of structural differences between these compounds. (NAc-dD-CHA-F-dS-dR-Y-L-W-S-βAla)$_2$-K-K(DOTA)-NH_2 is distinct from previously synthesized peptides in being N-terminally acetylated, C-terminally amidated, in the appended DOTA moiety C-terminal to the branching lysine residue, and in the chirality of the N-terminal aspartate residue.

The in vivo biodistribution of the ^{111}In-labeled peptide was compared with that of ^{125}I-labeled ATF, and was significantly different at all timepoints examined. At 1 and 4 hr pi, blood levels of each radiotracer were distinctly different, with the higher molecular weight ATF fragment demonstrating significantly slower clearance (Table 2, Table 3). ^{125}I-labeled ATF uptake was higher than (NAc-dD-CHA-F-dS-dR-Y-L-W-S-βAla)$_2$-K-K(^{111}In-DOTA)-NH_2 uptake in all normal tissues at these timepoints, with the exception of liver and kidney, which demonstrated higher levels of ^{111}In-peptide. Clearance of the ^{111}In-peptide occurs through both hepatobiliary and renal/urinary routes, and liver and kidney retention at 4 hr pi was higher than is usually observed for peptides in this molecular weight range (17–23). Increased liver and kidney retention is still observed for the ^{111}In-labeled branched peptide relative to ^{125}I-ATF at 24 hr pi, suggesting a structural mechanism of retention, perhaps due to the branched nature of this construct, distinct from normal residualization of ^{111}In-DOTA-amino acid conjugates.

With respect to specific retention of radiolabeled compounds in tumor tissue, significant ($p < 0.05$) blockade of ^{125}I-ATF uptake was only achieved at 24 hr pi, when tumor uptake was 34% blocked by pre-injection of 2 mg/kg unlabeled ATF 1 hr prior to injection of ^{125}I-ATF. Due to its more rapid clearance from blood and most normal tissues, (NAc-dD-CHA-F-dS-dR-Y-L-W-S-βAla)$_2$-K-K(^{111}In-DOTA)-NH_2 tumor uptake was significantly ($p < 0.05$) higher than that of the scrambled matched control peptide as early as 4 hr pi, with 47% higher uptake at this timepoint.

The peptide uPAR antagonist discussed in this work was originally synthesized as part of a combinatorial library of peptides targeting uPAR (15). This combinatorial library was synthesized to further search conformational space for highest affinity uPAR binders, using lead peptides derived from earlier bacteriophage peptide display libraries (14). One of these

peptides, termed AE105 in the original work (15), has served as the uPAR-targeting vector in two recent publications (16,17). In these studies, analogs of the AE105 parent peptide were N-terminally labeled with a DOTA moiety, with or without intervening linker residues, which served to coordinate imaging ^{64}Cu (17) or therapeutic ^{213}Bi (16). In the work described here, a dimeric peptide most closely related to AE120 in Ploug *et al*. (15) has been modified by addition of DOTA C-terminal to a branching lysine residue.

In the report by Knör *et al*. (16), the assembly of a dimeric construct resulted in increased specific binding of radiolabeled peptide to uPAR-expressing cells in vitro relative to N-terminally labeled linear monomeric peptides. This is in agreement with increased binding affinities of dimeric peptides reported originally in the development of this class of uPAR antagonists (15), although the radiopharmaceutical construct was unique in having an N-terminal, rather than C-terminal, branchpoint. Based on the higher affinity of a dimeric construct, Knör *et al*. subsequently used it in an in vivo model of human ovarian cancer, and demonstrated tumor uptake of the ^{213}Bi complex of 2.2 ± 0.4 %ID/g at 1.5 hr pi (16). This value is similar to the tumor uptake of 1.48 ± 0.28 at 1 hr pi described in this report, although the values are not directly comparable due to differences in model system, radioisotope, and experimental protocol. Additionally, the specificity of tumor uptake of the ^{213}Bi-labeled peptide in vivo was not addressed.

Li and co-workers have also recently published data relating to the use of radiolabeled uPAR antagonists for in vivo imaging of U87MG human glioma tumor xenografts (17). In this instance, an N-terminally DOTA-labeled AE105 analog was used to deliver the PET radionuclide ^{64}Cu to uPAR-expressing cells. In this instance, the DOTA chelating group was directly linked to the amino group of the N-terminal Laspartic acid residue of monomeric AE105. Tumor uptake in this model system was increased 2–5-fold relative to both the N-terminally modified dimeric construct of Knör *et al*. as well as the C-terminally modified dimeric construct described here (7.6 ± 0.9 %ID/g at 1 hr pi, as measured by PET imaging). Given the differences in experimental design among the three studies to date, more research will be required to directly compare these and similar analogs to define the optimal structure of uPAR-targeted molecular imaging agents.

One factor that could be responsible for differences in tumor uptake between different model cell lines is expression of endogenous uPA, resulting in blockade of available sites for binding of uPAR antagonists. The most widely used protocols for measurement of binding of radiolabeled uPAR ligands in vitro typically employ an acid stripping step, during which endogenously produced uPA is removed, thereby unmasking previously blocked uPAR. Knör and co-workers spoke to this issue by demonstrating tracer binding to OV-MZ-6 cells without prior acid stripping (16), suggesting that this cell line produces lower amounts of uPA than does the MDA-MB-231 line employed in this study. As shown in Figure 4 and Figure 5 in this work, binding of ^{125}I-ATF to MDA-MB-231 cells is increased when they have either had endogenous uPA removed by acid stripping (Fig. 4), or have had endogenous expression of uPA reduced by the application of specific siRNA's (Fig. 5). The fact that the increase in binding observed in figure 4 was seen following excision of MDA-MB-231 human tumor xenografts from SCID mice following 4–5 weeks of in vivo growth suggests that autocrine saturation could be responsible for reduced tumor uptake in vivo using this model system. Additionally, the MDA-MB-231 human breast cancer cell line is known to produce high levels of uPA, which has been proposed to be correlated with its high degree of invasiveness in in vitro assays (7,24). Lastly, the low specific tumor uptake of ^{125}I-ATF at 24 hr pi provides further evidence that the similarly low uptake of the ^{111}In-DOTA-peptide at 4 hr pi is not due solely to the lower affinity of the ^{111}In-labeled radiotracer, but is primarily the result of occupancy of uPAR sites within the tumor by endogenously expressed uPA.

uPA is a 54 kDa glycoprotein with well defined modular domains separated by a flexible linker region. Proteolysis of uPA yields a 36 kDa C-terminal domain that is catalytically active, plus an 18.5 kDa amino terminal fragment (ATF) that is responsible for binding to uPAR. The structure of ATF has been solved both by NMR and crystallographic methods (25,28). The ATF is itself composed of two independent domains, a C-terminal kringle domain attached via a flexible linker to an N-terminal growth factor-like domain (GFD). Receptor binding can be further localized within the ATF primarily to the GFD, within the N-terminal 45 amino acids of the ATF. The GFD shares significant homology to the epidermal growth factor (EGF), and binding of GFD to uPAR is mediated in large measure by a disulfide stabilized Ω loop region between residues 18–32 of the molecule. Numerous small peptides that behave as structural mimics of this receptor-binding region have been synthesized and characterized (14–17,26, 28,29), including the lead peptide composing the targeting moiety of the construct described here.

The development of low molecular weight uPAR antagonists as imaging agents for the detection of uPAR-expressing malignancies will potentially have relevance both to patient stratification and therapy monitoring. Several different approaches to cancer therapy have been described that target elements of the urokinase-type plasminogen activator system. These include inhibition of uPA enzymatic activity (30), blockade of uPA/uPAR binding (14,15), targeted delivery of therapeutic radionuclides to uPAR-expressing tumors (16), and RNA interference (31). Targeted knockdown of uPA by a variety of methods, including delivery of siRNA's, shRNA's, or antisense RNA's, is currently under active investigation for cancer therapy (24,31,32). Such reductions in in vivo expression of uPA have been shown to reduce the metastatic potential of tumor cells and to reduce the rate of tumor growth. In the context of uPA-targeted RNA interference, imaging agents such as the type described here could provide a direct measure of treatment efficacy in vivo, by generating increasing signal proportional to the degree of uPA knockdown. With respect to blockade of uPA/uPAR binding, such a probe could facilitate delivery of inhibitors by enabling real-time monitoring of dosages required for inhibition of probe signal generation. Probes of the type illustrated here could ultimately provide a complementary imaging modality to optical sensors of uPA activity currently under development (33,34). Further experiments are currently underway to develop the correlation suggested here between receptor occupancy and radiotracer uptake in vivo.

Acknowledgments

This material is the result of work supported with resources and the use of facilities at the Harry S. Truman Memorial Veterans' Hospital, Columbia, MO, 65201 and the Department of Radiology, University of Missouri-Columbia School of Medicine, Columbia, MO 65211. This work was funded by a United States Department of Veterans' Affairs Biomedical Laboratory Research and Development Service VA Merit Award, a National Cancer Institute Center grant (1 P50 CA103130-01), and a United States Department of Defense Concept Award (BC032697).

References

1. Blasi F, Carmeliet P. uPAR: a versatile signaling orchestrator. Nat. Rev. Mol. Cell Biol 2002;3:932–943. [PubMed: 12461559]
2. Ploug M. Structure-function relationships in the interaction between the urokinase-type plasminogen activator and its receptor. Curr. Pharm. Des 2003;9:1499–1528. [PubMed: 12871065]
3. Romer J, Nielsen BS, Ploug M. The urokinase receptor as a potential target in cancer therapy. Curr. Pharm. Des 2004;10:2359–2376. [PubMed: 15279614]
4. Danø K, Behrendt N, Høyer-Hansen G, Johnsen M, Lund LR, Ploug M, Rømer J. Plasminogen activation and cancer. Thromb. Haemost 2005;93:676–681. [PubMed: 15841311]
5. Xue A, Scarlett CJ, Jackson CJ, Allen BJ, Smith RC. Prognostic significance of growth factors and the urokinase-type plasminogen activator system in pancreatic ductal adenocarcinoma. Pancreas 2008;36:160–167. [PubMed: 18376307]

6. Beyer BC, Heiss MM, Simon EH, Gruetzner KU, Babic R, Jauch KW, Schildberg FW, Allgayer H. Urokinase system expression in gastric carcinoma: prognostic impact in an independent patient series and first evidence of predictive value in preoperative biopsy and intestinal metaplasia specimens. Cancer 2006;106:1026–1035. [PubMed: 16435385]
7. Holst-Hansen C, Johannessen B, Hoyer-Hansen G, Romer J, Ellis V, Brunner N. Urokinase-type plasminogen activation in three human breast cancer cell lines correlates with their in vitro invasiveness. Clin. Exp. Metastasis 1996;14:297–307. [PubMed: 8674284]
8. Boyd DD, Kim S, Wang H, Jones TR, Gallick GE. A urokinasederived peptide (A6) increases survival of mice bearing orthotopically grown prostate cancer and reduces lymph node metastasis. Am. J. Pathol 2003;162:619–626. [PubMed: 12547719]
9. Boyd DD, Wang H, Avila H, Parikh NU, Kessler H, Magdolen V, Gallick GE. Combination of an SRC kinase inhibitor with a novel pharmacological antagonist of the urokinase receptor diminishes in vitro colon cancer invasiveness. Clin. Cancer Res 2004;10:1545–1555. [PubMed: 14977859]
10. Yang L, Avila H, Wang H, Trevino J, Gallick GE, Kitadai Y, Sasaki T, Boyd DD. Plasticity in urokinase-type plasminogen activator receptor (uPAR) display in colon cancer yields metastable subpopulations oscillating in cell surface uPAR density--implications in tumor progression. Cancer Res 2006;66:7957–7967. [PubMed: 16912170]
11. Foekens JA, Peters HA, Look MP, Portengen H, Schmitt M, Kramer MD, Brünner N, Jänicke F, Meijer-van Gelder ME, Henzen-Logmans SC, van Putten WL, Klijn JG. The urokinase system of plasminogen activation and prognosis in 2780 breast cancer patients. Cancer Res 2000;60:636–643. [PubMed: 10676647]
12. Reuning U, Sperl S, Kopitz C, Kessler H, Krüger A, Schmitt M, Magdolen V. Urokinase-type plasminogen activator (uPA) and its receptor (uPAR): development of antagonists of uPA/uPAR interaction and their effects in vitro and in vivo. Curr. Pharm. Des 2003;9:1529–1543. [PubMed: 12871066]
13. Stoppelli MP, Corti A, Soffientini A, Cassani G, Blasi F, Assoian RK. Differentiation-enhanced binding of the amino-terminal fragment of human urokinase plasminogen activator to a specific receptor on U937 monocytes. Proc. Natl. Acad. Sci. U.S.A 1985;82:4939–4943. [PubMed: 2991901]
14. Goodson RJ, Doyle MV, Kaufman SE, Rosenberg S. High-affinity urokinase receptor antagonists identified with bacteriophage peptide display. Proc. Natl. Acad. Sci. U.S.A 1994;91:7129–7133. [PubMed: 8041758]
15. Ploug M, Ostergaard S, Gardsvoll H, Kovalski K, Holst-Hansen C, Holm A, Ossowski L, Dano K. Peptide-derived antagonists of the urokinase receptor. affinity maturation by combinatorial chemistry, identification of functional epitopes, and inhibitory effect on cancer cell intravasation. Biochemistry 2001;40:12157–12168. [PubMed: 11580291]
16. Knör S, Sato S, Huber T, Morgenstern A, Bruchertseifer F, Schmitt M, Kessler H, Senekowitsch-Schmidtke R, Magdolen V, Seidl C. Development and evaluation of peptidic ligands targeting tumour-associated urokinase plasminogen activator receptor (uPAR) for use in alpha-emitter therapy for disseminated ovarian cancer. Eur. J. Nucl. Med. Mol. Imaging 2008;35:53–64. [PubMed: 17891393]
17. Li Z, Niu G, He L, Yang L, Ploug M, Chen X. Imaging of urokinase-type plasminogen activator receptor expression using a 64Cu-labeled linear peptide antagonist by microPET. Clin. Cancer Res 2008;14:4758–4766. [PubMed: 18676745]
18. Thakur ML, Aruva MR, Gariepy J, Acton P, Rattan S, Prasad S, Wickstrom E, Alavi A. PET imaging of oncogene overexpression using ^{64}Cu-vasoactive intestinal peptide (VIP) analog: comparison with ^{99m}Tc-VIP analog. J. Nucl. Med 2004;45:1381–1389. [PubMed: 15299065]
19. Hoffman TJ, Gali H, Smith CJ, Sieckman GL, Hayes DL, Owen NK, Volkert WA. Novel series of ^{111}In-labeled bombesin analogs as potential radiopharmaceuticals for specific targeting of gastrin-releasing peptide receptors expressed on human prostate cancer cells. J. Nucl. Med 2003;44:823–831. [PubMed: 12732685]
20. Giblin MF, Gali H, Sieckman GL, Owen NK, Hoffman TJ, Forte LR, Volkert WA. In vitro and in vivo comparison of human Escherichia coli heat-stable peptide analogues incorporating the ^{111}In-DOTA group and distinct linker moieties. Bioconj. Chem 2004;15:872–880.

21. Giblin MF, Wang N, Hoffman TJ, Jurisson SS, Quinn TP. Design and characterization of alpha-melanotropin peptide analogs cyclized through rhenium and technetium metal coordination. Proc. Natl. Acad. Sci. U.S.A 1998;95:12814–12818. [PubMed: 9788997]
22. Storch D, Béhé M, Walter MA, Chen J, Powell P, Mikolajczak R, Mäcke HR. Evaluation of [^{99m}Tc/EDDA/HYNIC0]octreotide derivatives compared with [^{111}In-DOTA0,Tyr3, Thr8]octreotide and [^{111}In-DTPA0]octreotide: does tumor or pancreas uptake correlate with the rate of internalization? J. Nucl. Med 2005;46:1561–1569. [PubMed: 16157541]
23. Wu Y, Zhang X, Xiong Z, Cheng Z, Fisher DR, Liu S, Gambhir SS, Chen X. microPET imaging of glioma integrin {alpha}v{beta}3 expression using (64)Cu-labeled tetrameric RGD peptide. J. Nucl. Med 2005;46:1707–1718. [PubMed: 16204722]
24. Arens N, Gandhari M, Bleyl U, Hildenbrand R. In vitro suppression of urokinase plasminogen activator in breast cancer cells--a comparison of two antisense strategies. Int. J. Oncol 2005;26:113–119. [PubMed: 15586231]
25. Hansen AP, Petros AM, Meadows RP, Nettesheim DG, Mazar AP, Olejniczak ET, Xu RX, Pederson TM, Henkin J, Fesik SW. Solution structure of the amino-terminal fragment of urokinase-type plasminogen activator. Biochemistry 1994;33:4847–4864. [PubMed: 8161544]
26. Guthaus E, Schmiedeberg N, Burgle M, Magdolen V, Kessler H, Schmitt M. The urokinase receptor (uPAR, CD87) as a target for tumor therapy: uPAsilica particles (SP-uPA) as a new tool for assessing synthetic peptides to interfere with uPA/uPA-receptor interaction. Recent Results Cancer Res 2003;162:3–14. [PubMed: 12790317]
27. Appella E, Robinson EA, Ullrich SJ, Stoppelli MP, Corti A, Cassani G, Blasi F. The receptor-binding sequence of urokinase. A biological function for the growth-factor module of proteases. J. Biol. Chem 1987;262:4437–4440. [PubMed: 3031025]
28. Huai Q, Mazar AP, Kuo A, Parry GC, Shaw DE, Callahan J, Li Y, Yuan C, Bian C, Chen L, Furie B, Furie BC, Cines DB, Huang M. Structure of human urokinase plasminogen activator in complex with its receptor. Science 2006;311:656–659. [PubMed: 16456079]
29. Llinas P, Le Du MH, Gårdsvoll H, Danø K, Ploug M, Gilquin B, Stura EA, Ménez A. Crystal structure of the human urokinase plasminogen activator receptor bound to an antagonist peptide. EMBO J 2005;24:1655–1663. [PubMed: 15861141]
30. Setyono-Han B, Stürzebecher J, Schmalix WA, Muehlenweg B, Sieuwerts AM, Timmermans M, Magdolen V, Schmitt M, Klijn JG, Foekens JA. Suppression of rat breast cancer metastasis and reduction of primary tumour growth by the small synthetic urokinase inhibitor WX-UK1. Thromb. Haemost 2005;93:779–786. [PubMed: 15841327]
31. Pulukuri SM, Gondi CS, Lakka SS, Jutla A, Estes N, Gujrati M, Rao JS. RNA interference-directed knockdown of urokinase plasminogen activator and urokinase plasminogen activator receptor inhibits prostate cancer cell invasion, survival, and tumorigenicity in vivo. J. Biol. Chem 2005;280:36529–36540. [PubMed: 16127174]
32. Mohanam S, Jasti SL, Kondraganti SR, Chandrasekar N, Kin Y, Fuller GN, Lakka SS, Kyritsis AP, Dinh DH, Olivero WC, Gujrati M, Yung WK, Rao JS. Stable transfection of urokinase-type plasminogen activator antisense construct modulates invasion of human glioblastoma cells. Clin. Cancer Res 2001;7:2519–2526. [PubMed: 11489835]
33. Law B, Curino A, Bugge TH, Weissleder R, Tung CH. Design, synthesis, and characterization of urokinase plasminogen-activator-sensitive nearinfrared reporter. Chem. Biol 2004;11:99–106. [PubMed: 15112999]
34. Law B, Weissleder R, Tung CH. Protease-sensitive fluorescent nanofibers. Bioconj. Chem 2007;18:1701–1704.

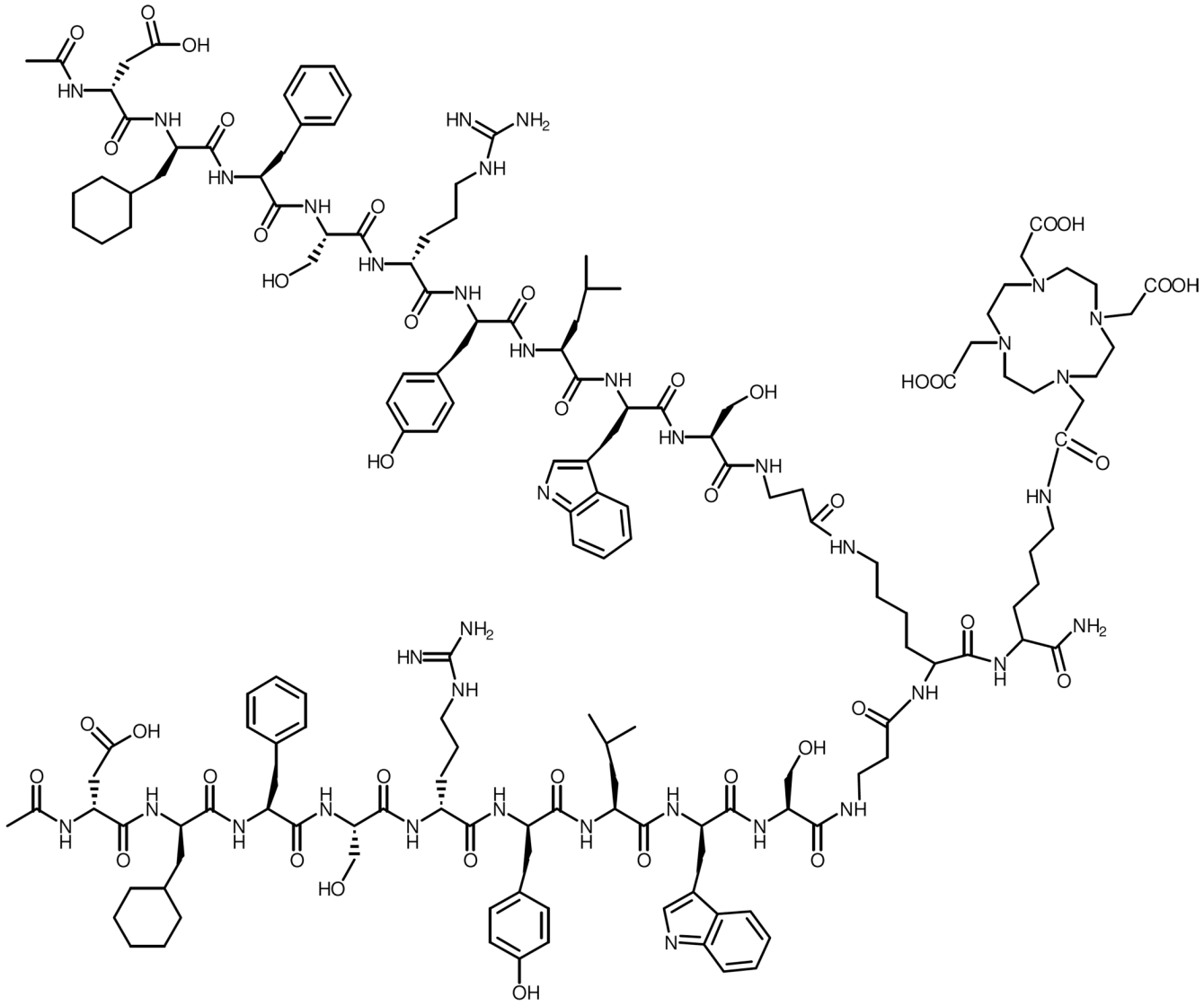

Figure 1.
Structure of (NAc-dD-CHA-F-dS-dR-Y-L-W-S-βAla)$_2$-K-K(DOTA)-NH$_2$

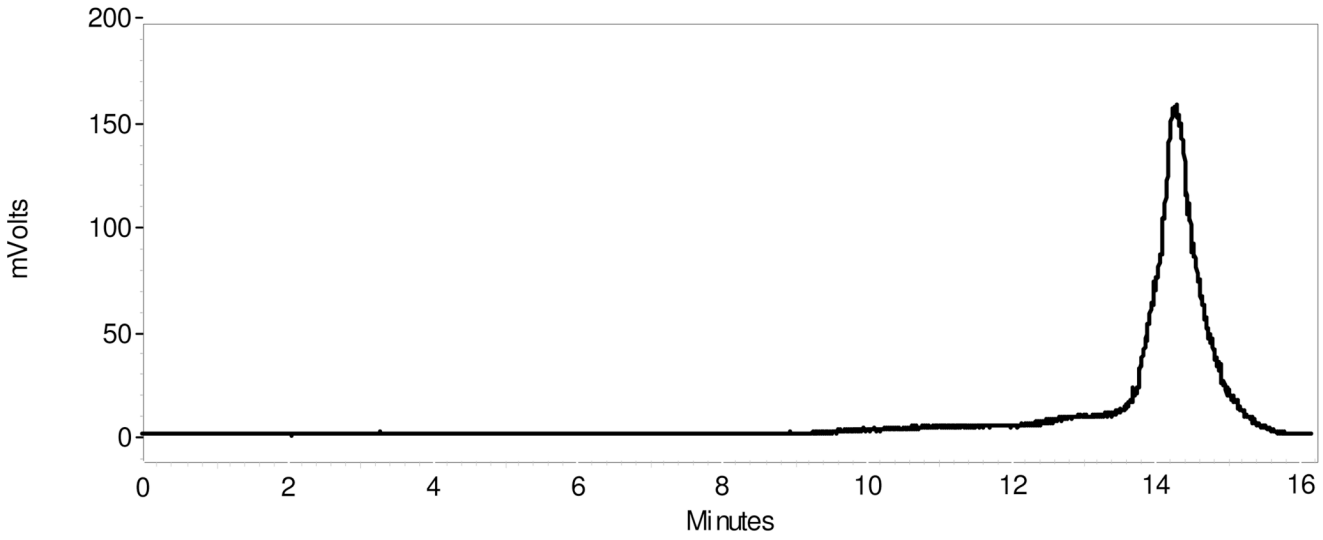

Figure 2.
HPLC chromatogram of purified (NAc-dD-CHA-F-dS-dR-Y-L-W-S-βAla)$_2$-K-K(^{111}In-DOTA)-NH_2. The ^{111}In-peptide elutes at 14.1 minutes, while the unlabeled peptide has a retention time of 13.6 minutes.

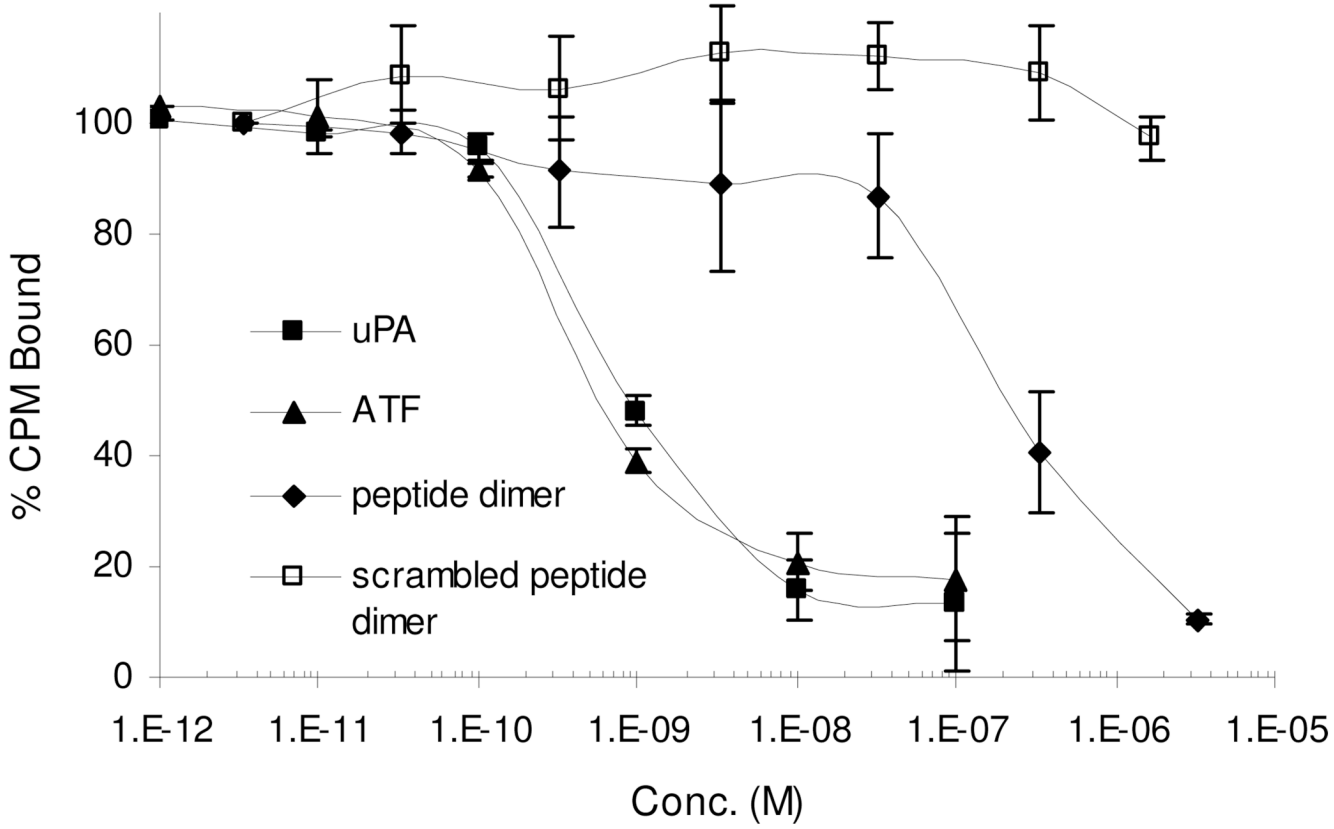

Figure 3.
Competitive receptor binding assay using intact MDA-MB-231 human breast cancer cells and ^{125}I-ATF.

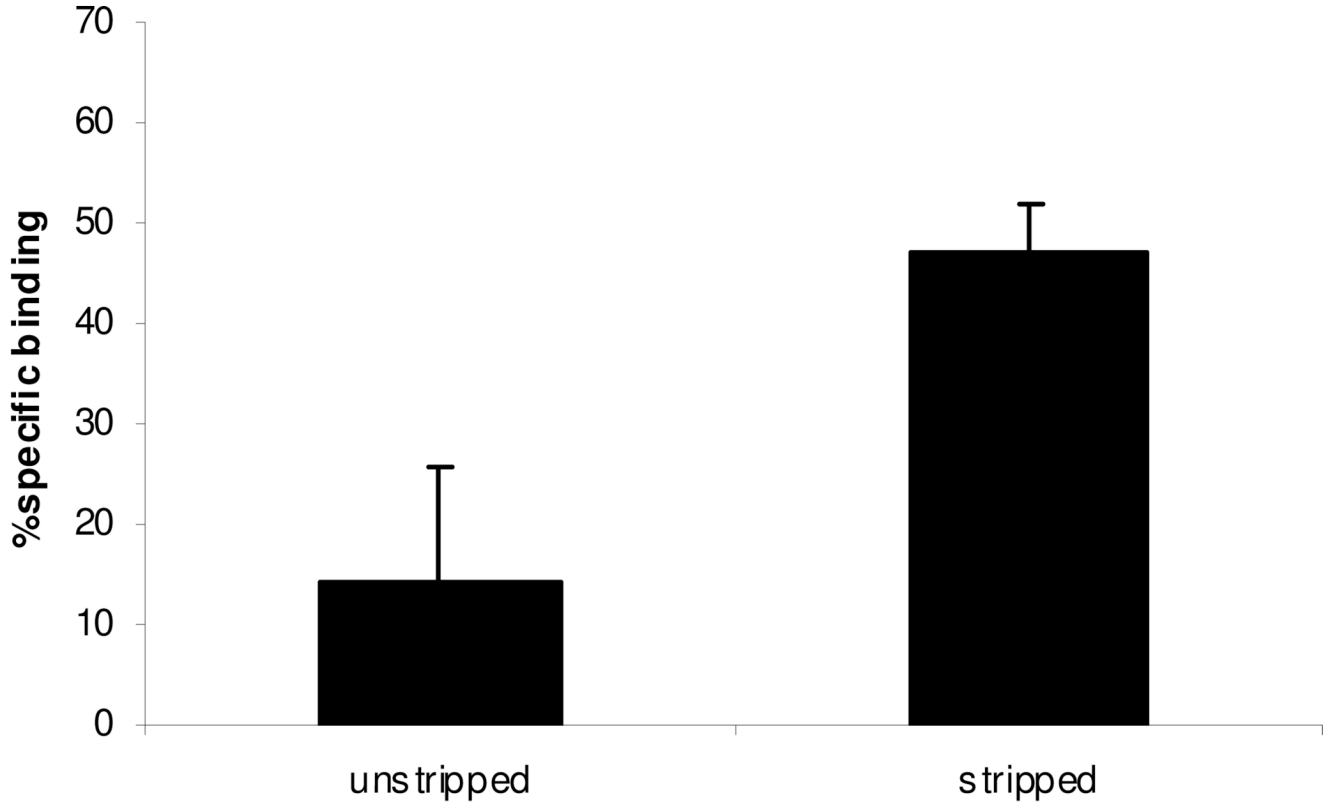

Figure 4.

Specific binding of ^{125}I-ATF to MDA-MB-231 tumor cells ex vivo. MDA-MB-231 tumor xenografts were harvested from SCID mice following 4–6 weeks of in vivo growth. Tumors were physically dissociated in a buffered collagenase solution, and specific binding of ^{125}I-ATF was measured using either native preparations or cell preparations stripped of endogenous uPA with pH 3.0 buffer.

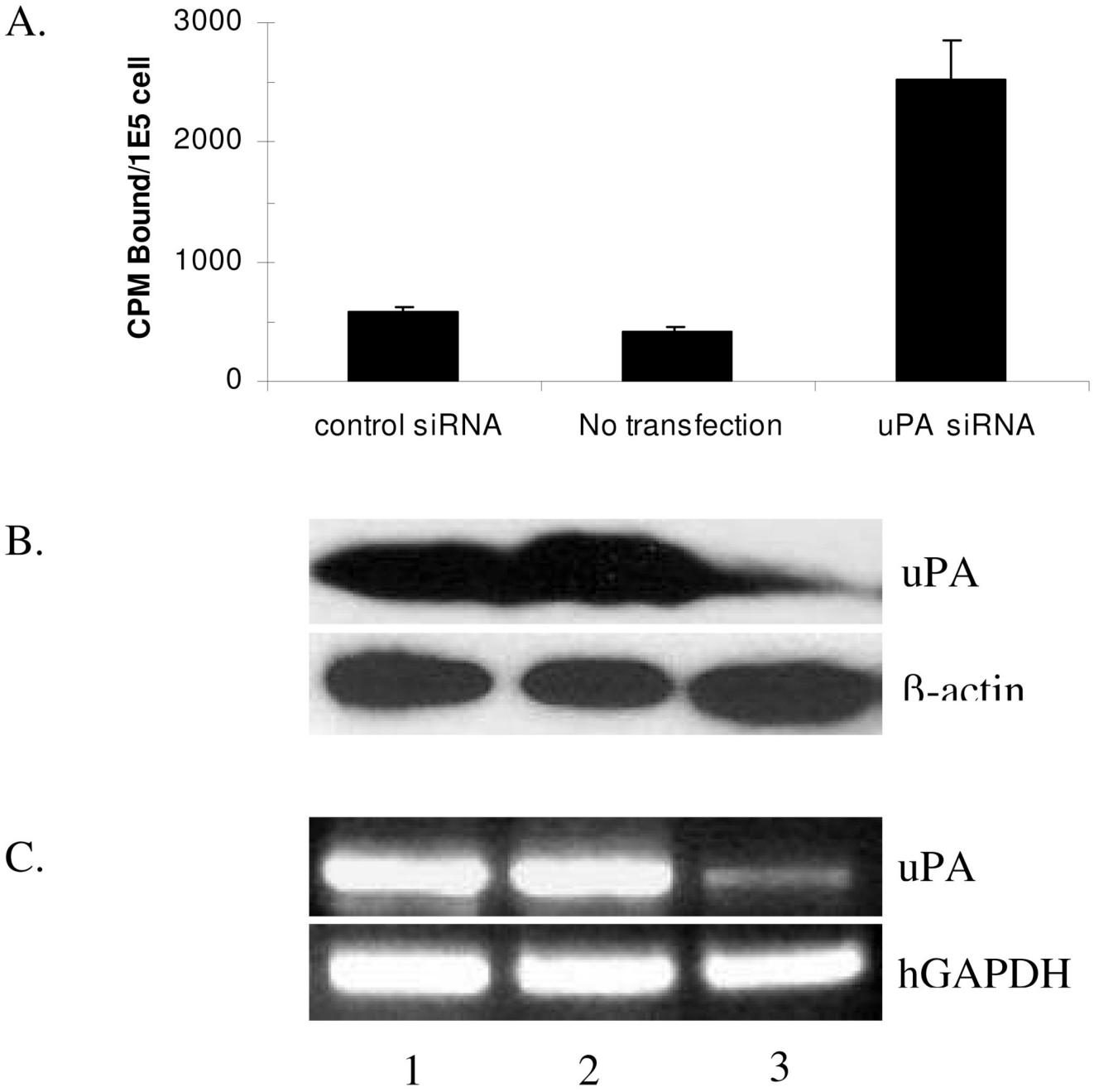

Figure 5.

A. Binding of ^{125}I-ATF to MDA MB-231 cells following knockdown of endogenous uPA production using a uPA-specific set of siRNA's. B. Western blot demonstrating uPA knockdown 2 days post-transfection of MDA-MB-231 cells. C. RTPCR demonstrating decreased uPA message in siRNA transfected MDA-MB-231 cells. Lane 1, control siRNA; lane 2, no-transfection; lane 3, uPA siRNA.

Table 1

Calculated and observed molecular weights and IC_{50} values of DOTA-peptides.

Peptide	$(M+H)^+$ Calc.	$(M+H)^+$ Obs.	IC_{50} (nM)
(NAc-dD-CHA-F-dS-dR-YLWS-βAla)$_2$-K-K(DOTA)-NH_2	3301.5	3301.7	240 ± 125
(NAc-dD-W-dS-LY-dR-FS-CHA-βAla)$_2$-K-K(DOTA)-NH_2	3301.5	3301.7	--

Table 2

In vivo biodistribution of (NAc-dD-CHA-F-dS-dR-Y-L-W-S-βAla)$_2$-K-K(^{111}In-DOTA)-NH_2 ("Test") at 1, 4, and 24 hr post injection and scrambled negative control peptide (NAc-dD-W-dS-L-Y-dR-F-S-CHA-βAla)$_2$-K-K(^{111}In-DOTA)-NH_2 ("Control") at 4 hr post injection in SCID mice bearing MDA-MB-231 human breast cancer tumor xenografts (N=3, mean %ID/g ± SD).

Organ	Test 1 hr	Test 4 hr	Control 4 hr	Test 24 hr
Blood	2.85 ± 0.57	0.12 ± 0.06	0.15 ± 0.04	0.07 ± 0.02
Heart	0.93 ± 0.22	0.16 ± 0.02	0.55 ± 0.08	0.10 ± 0.03
Lung	2.58 ± 0.51	0.42 ± 0.18	0.32 ± 0.06	0.32 ± 0.05
Liver	7.97 ± 0.70	5.52 ± 0.95	13.44 ± 1.57	4.06 ± 0.34
Spleen	0.72 ± 0.18	0.39 ± 0.34	0.37 ± 0.09	0.41 ± 0.04
Intestines	1.07 ± 0.06	1.74 ± 1.09	1.71 ± 0.38	0.23 ± 0.07
Kidney	19.09 ± 0.97	13.27 ± 2.61	13.19 ± 3.18	10.23 ± 2.29
Muscle	0.30 ± 0.08	0.06 ± 0.02	0.12 ± 0.02	0.03 ± 0.01
Bone	0.49 ± 0.22	0.06 ± 0.04	0.09 ± 0.02	0.06 ± 0.05
Pancreas	0.83 ± 0.26	0.15 ± 0.07	0.25 ± 0.03	0.07 ± 0.06
Tumor	1.48 ± 0.28	0.53 ± 0.11	0.36 ± 0.05	0.23 ± 0.07

Table 3

In vivo biodistribution (N=3, mean %ID/g ± SD) of ^{125}I-ATF in SCID mice bearing MDA-MB-231 human breast cancer tumor xenografts at 1, 4, and 24 hr post injection.

Organ	1 hr	4 hr	24 hr	24 hr (blocked)
Blood	7.75 ± 1.00	3.41 ± 0.86	0.26 ± 0.06	0.60 ± 0.69
Heart	2.56 ± 0.12	1.19 ± 0.16	0.08 ± 0.02	0.06 ± 0.01
Lung	5.39 ± 0.35	2.67 ± 0.51	0.16 ± 0.05	0.17 ± 0.02
Liver	3.01 ± 0.45	1.81 ± 0.42	0.25 ± 0.06	0.23 ± 0.02
Spleen	2.92 ± 0.39	1.72 ± 0.35	0.09 ± 0.02	0.10 ± 0.03
Intestines	3.27 ± 0.40	2.53 ± 0.28	0.16 ± 0.03	0.13 ± 0.02
Kidney	16.72 ± 1.59	4.65 ± 0.84	0.88 ± 0.21	0.81 ± 0.09
Muscle	1.21 ± 0.08	0.61 ± 0.10	0.03 ± 0.01	0.02 ± 0.01
Bone	1.55 ± 0.13	0.87 ± 0.11	0.04 ± 0.01	0.03 ± 0.001
Pancreas	3.98 ± 0.77	2.18 ± 0.65	0.06 ± 0.03	0.05 ± 0.01
Tumor	4.60 ± 0.63	3.09 ± 0.29	0.29 ± 0.06	0.19 ± 0.05